Title

Photomediated ring contraction of saturated heterocycles

Journal

Science, 373(6558)

ISSN

0036-8075

Authors

Jurczyk, Justin
Lux, Michaelyn C
Adpressa, Donovon
et al.

Publication Date

2021-08-27

DOI

10.1126/science.abi7183

Peer reviewed

HHS Public Access

Author manuscript

Science. Author manuscript; available in PMC 2021 November 27.

Published in final edited form as:

Science. 2021 August 27; 373(6558): 1004–1012. doi:10.1126/science.abi7183.

Photomediated ring contraction of saturated heterocycles

Justin Jurczyk[1,†], **Michaelyn C. Lux**[2,†], **Donovon Adpressa**[3], **Sojung F. Kim**[1], **Yu-hong Lam**[4,*], **Charles S. Yeung**[2,*], **Richmond Sarpong**[1,*]

[1]Department of Chemistry, University of California, Berkeley, CA 94720, USA.

[2]Discovery Chemistry, Merck & Co., Inc., Boston, MA 02115, USA.

[3]Analytical Research and Development, Merck & Co. Inc., Boston, MA 02115, USA.

[4]Computational and Structural Chemistry, Merck & Co. Inc., Rahway, NJ 07065, USA.

Abstract

Saturated heterocycles are found in numerous therapeutics and bioactive natural products and are abundant in many medicinal and agrochemical compound libraries. To access new chemical space and function, many methods for functionalization on the periphery of these structures have been developed. Comparatively fewer methods are known for restructuring their core framework. Herein, we describe a visible light–mediated ring contraction of α-acylated saturated heterocycles. This unconventional transformation is orthogonal to traditional ring contractions, challenging the paradigm for diversification of heterocycles including piperidine, morpholine, thiane, tetrahydropyran, and tetrahydroisoquinoline derivatives. The success of this Norrish type II variant rests on reactivity differences between photoreactive ketone groups in specific chemical environments. This strategy was applied to late-stage remodeling of pharmaceutical derivatives, peptides, and sugars.

Saturated heterocycles, especially piperidines, are among the most frequently encountered scaffolds in biologically active small molecules (1, 2). The prevalence of the piperidine scaffold in pharmaceutical and agrochemical compound libraries has resulted in increased interest in the development of methods for its site-selective derivatization (Fig. 1A) to access new chemical space. Recent advancements in C(sp^3)–H functionalization have provided many powerful methods for peripheral functionalization of the piperidine framework (3–12), shifting the paradigm in late-stage functionalization. By comparison, methods that modify the piperidine skeleton are less abundant, prompting a quest for methods for this purpose.

*Corresponding author. yu.hong.lam@merck.com (Y.-h.L.); charles.yeung@merck.com (C.S.Y.); rsarpong@berkeley.edu (R.S.).

Author contributions: J.J., M.C.L., C.S.Y., and R.S. conceived and designed the experiments reported in this work. J.J., M.C.L., and S.F.K. performed all laboratory experiments. D.A. assisted in structural elucidation. Y.-h.L. designed and completed the DFT calculations. J.J., M.C.L., S.F.K., Y.-h.L., C.S.Y., and R.S. wrote the manuscript. C.S.Y. and R.S. directed the research.

†These authors contributed equally to this work.

Competing interests: R.S. is a paid consultant for MSD. The authors declare no other competing interests.

SUPPLEMENTARY MATERIALS

science.sciencemag.org/content/373/6558/1004/suppl/DC1

Materials and Methods

Figs. S1 to S30

Tables S1 to S7

References (49–69)

Such methods would be especially valuable for drug discovery, in which maximizing structural diversity, specifically at a late stage, is highly valued (13). To this end, we sought to develop a ring contraction of piperidines and related saturated heterocycles to carbocyclic frameworks to achieve core, rather than peripheral, modification.

Relatively few methods for piperidine ring contraction exist compared with those available for the ring contraction of carbocycles bearing functional handles. For example, in cyclohexanone derivatives alone, anionic, carbene, and cationic intermediates have all been exploited to achieve ring contraction. By contrast, for saturated nitrogen–containing heterocycles (azacycles), commonly used ring contraction strategies predominantly leverage bicyclic, quaternary-ammonium intermediates, which undergo a formal ring contraction upon attack from an exogenous nucleophile (Fig. 1B) (14, 15). More recently, we reported an approach for piperidine ring contraction through oxidative C(sp^3)–N bond cleavage, wherein silver-mediated deconstructive bromination of *N*-benzoyl piperidines followed by intramolecular C–N bond reformation in the resulting acyclic bromoamine furnishes the corresponding *N*-benzoyl pyrrolidine scaffolds in two steps (Fig. 1B) (16). Although useful, these tactics are limited to piperidine-to-pyrrolidine scaffold conversions, require specific substitution patterns (14, 15), and use strongly oxidizing conditions that pose a challenge for late-stage diversification (16, 17). The ring contractions of unsaturated azacyclic systems such as pyridiniums and dihydropyridines have also been explored, for example, by using light (18, 19). However, these transformations are limited to substrates with well-recognized photoreactivity profiles.

We sought to develop a complementary and mechanistically distinct approach to piperidine ring contraction that could also be applied to a wide range of saturated heterocycles to provide access to underexplored, skeletally diverse substrates. We drew inspiration from an unusual transformation reported by Seebach and co-workers (Fig. 1C), in which an α-carboxyl tetrahydroisoquinoline (THIQ) derivative (**1a**) underwent contraction to the corresponding indane scaffold (**2a**) under strongly basic conditions. This transformation features a curious endo-to-exocyclic nitrogen atom transposition, giving rise to a β–amino acid structural motif (20). Despite its novelty, only two examples were reported, and the requisite strongly basic conditions limit its potential application to skeletal modification of drug-like molecules bearing base-reactive functional groups. A more functional-group-compatible, albeit similarly specific, variant of this type of transformation was reported by Suárez and co-workers for α-diketonyl sugars (e.g., **1b**), which undergo light-mediated ring contraction with a subsequent hemiketalization to give fused [5,5] ring systems (i.e., **2b**) (Fig. 1D) (21, 22). Notably, the α-diketone moiety required for the reaction is derivatized in the resulting product. Our design of a complementary ring contraction sought broad functional group compatibility and a widened scope beyond α-diketonyl-derived sugars. Herein, we report the visible light–mediated ring contraction of α-acylated cyclic piperidines to furnish *cis*-1,2–disubstituted cyclopentane scaffolds (Fig. 1E) and the extension of this method to other saturated heterocycles including tetrahydropyrans and thianes. The success of these Norrish type II transformations hinged on predicted (and observed) photophysical differences between the ketone groups in the starting substrates and products (vide infra). An asymmetric variant of this transformation is also described.

Development of photomediated ring contraction

We commenced our studies by focusing on piperidine ring contractions (Fig. 2A). We envisioned that upon irradiation, α-acylated precursors such as **I**, in which the aroyl group is disposed pseudoaxially to avoid pseudo $A^{1,3}$-like strain (23), would undergo excitation and intersystem crossing to afford **II** in the triplet state. A subsequent Norrish type II 1,5-hydrogen atom transfer (HAT) would yield the corresponding 1,4-diradical (**III**), which would undergo homolytic C–N bond fragmentation, leading to imine-enol **IV**. The desired cyclopentane product would then result from an intramolecular enol attack on the tethered imine (Mannich reaction) to afford cyclopentane **V**. Under photoirradiation, however, we also recognized the potential for undesired reactivity (Fig. 2B), especially further reactivity of the reaction product (**V**) to form additional excited species such as **VI**.

In principle, the success of the reaction would depend on subtle differences in reactivity between the starting material (**I**) and the reaction product (**V**; an anticipated "photostationary" state), because both bear a photoreactive phenyl ketone that could participate in Norrish-type processes (see **VI**). In their studies (Fig. 1D), Suárez and co-workers had achieved success primarily because a photostationary state was reached upon hemiketalization of the α-diketone in the product (21, 22). We envisioned that even though chemical transformation of the photoreactive moiety would not be realized upon product formation in our case, differences in the n→π* photoabsorption profiles of **I** and **V** could arise by virtue of an intramolecular H-bond that is established in **V**. As is well known for spatially forbidden n→π* transitions, increased polarity in the local environment can lead to a hypsochromic (blue) shift for λ_{max} (24), which we anticipated would lead to differences in the photoreactivity of **I** and **V**. Additionally, we recognized that other photochemical processes could outcompete our desired ring contraction reaction. For example, although more prominent for dialkyl ketones, Norrish type I C–C bond homolysis from the triplet excited state (i.e., **II**) could lead to the formation of undesired alkyl-acyl radical pairs (see **VII**) (24). Another possible complication could arise after 1,5-hydrogen atom abstraction, in which radical recombination of diradical **III** could occur to give the corresponding [3.1.1]-bicycle (**VIII**), i.e., a Norrish–Yang cyclization. We imagined that a Norrish type **II** C–N fragmentation of **III** (to ultimately afford **V**) would outcompete a Norrish–Yang cyclization on the basis of an anticipated unfavorable conformational bias against ring closure to azetidinol **VIII** and a slower rate for intersystem crossing to the requisite singlet diradical for cyclobutanol C–C bond formation (25).

Despite the potential challenges associated with side reactions and overreactions of our phenyl ketone substrate, on the basis of the anticipated differences in absorptivity for **I** and **V**, we reasoned that tuning the wavelength of light could selectively promote the desired reactivity while minimizing the photoreactivity of the resulting products. Gratifyingly, photoirradiation of **3a** using a 400-nm blue LED lamp provided 1,2-disubstituted cyclopentane **4a** in 73% yield at room temperature (Fig. 2C, entry 1). Empirically, the photomediated ring contraction proceeded best with a 400-nm-wavelength light source; longer wavelength irradiation (centered at 450 nm; lower energy) did not result in any conversion, whereas shorter wavelength light sources (e.g., centered at 385 nm; higher energy), which more closely aligned with the calculated and measured absorptivity curves of

both product and starting material, led to competing nonspecific oligomerization. Sulfonyl groups on the piperidine nitrogen were especially effective in providing the desired product in good to high yields, presumably enhancing the intramolecular H-bond in **4a** that accounts for its stability under the reaction conditions. Other electron-withdrawing groups on the piperidine nitrogen, such as benzoyl, Boc, or pivaloyl (Fig. 2C, entries 2 to 4), resulted in lower yields of the ring contraction product. The choice of solvent was also critical. Benzene, which can enhance H-bonding in **4a**, gave the highest yields and diastereoselectivity (26). Other solvents, such as methanol (Fig. 2C, entry 5), acetonitrile (Fig. 2C, entry 6), toluene (Fig. 2C, entry 7), and trifluorotoluene (Fig. 2C, entry 8), led to diminished yields and lower diastereoselectivity. Given the toxicity concerns of using benzene, we have also identified *p*-xylene as a serviceable solvent alternative (Fig. 2C, entry 9; see the supplementary materials for full solvent screen, and select substrates using *p*-xylene as the solvent). Lowering the concentration of the substrate also led to improvements in yield; a concentration of 0.05 M, which presumably slows the rate of competing unproductive intermolecular side reactions, was determined to be optimal. From these observations, we identified an optimized set of conditions for sulfonyl derivatives of the piperidine substrates, which afforded **4a** in 84% isolated yield and high diastereoselectivity (Fig. 2C, entry 13). The reaction could be performed at gram scale under continuous (flow) conditions (Fig. 2C, entry 14; see the supplementary materials for additional details). For substrates bearing other protecting groups, such as amide and carbamate substrates, we observed reduced conversion to the desired product. This observation was intriguing because, ostensibly, the photoreactive phenyl ketone group in the starting substrates was conserved. We posited that changing the group on nitrogen (e.g., sulfonyl to acyl or carbamoyl) could lead to discrete differences in the triplet state energy of the phenyl ketone. We hypothesized that a photosensitizer or photocatalyst could improve the efficacy of the reaction, and thus we initiated a screen of 46 known photosensitizers and photocatalysts using amide substrate **3n**. 3-Cyanoumbelliferone (**IX**; Fig. 2C, entry 16) emerged as an effective additive that improved the efficiency of the reaction: Piperidine **3m**, **3o**, **3s**, and **3t** were converted to their corresponding cyclopentylamines with improved yields (average of 11% increase, vide infra). The observed effect appeared to be subtle and substrate dependent. Efforts to further understand the role of cyanoumbelliferone **IX** are ongoing.

Scope of the photomediated ring contraction

With optimized conditions in hand, the scope of the visible-light mediated ring contraction was explored (Fig. 3A). The generality of the group on the nitrogen atom was investigated first. Arylsulfonyl-derivatized piperidines featuring electron-withdrawing substituents, such as ketones (e.g., **3h**), esters (e.g., **3i**), and halogens (**3e** to **3g**), led to good to modest yields of the respective ring-contracted products. Likewise, arylsulfonyl-derivatized piperidines bearing electron-donating groups such as ethers (e.g., **3c** and **3d**) were also competent in the ring contraction transformation. The presence of a *p*-nitro substituent (**3j**) resulted in the complete recovery of starting material, likely resulting from photoquenching (27–29). Although arylsulfonyl substituents on the piperidine nitrogen led to the highest ring contraction product yields, substrates bearing acyl (e.g., **3m** to **3p**), carbamoyl (**3q**), and

urea-type groups (e.g., **3r** and **3s**) on the nitrogen also led to successful ring contraction in the presence of cyanoumbelliferone (**IX**) (Fig. 3A).

Phosphoramidite-containing substrates (**3t** and **3u**) were also competent, providing the cyclopentane products in yields comparable to those observed for substrates bearing a sulfonyl group. In these cases, the phosphoramidyl group is easily removed under acidic conditions (30). The efficacy of the additive was also found to vary depending on the substrate, with the conversion of **3q** to **4q** being minimally affected upon adding **IX**. Here, the persisting low yield likely involves reduced productive hydrogen atom transfer because of a preference for an unproductive conformation of the starting material (see the supplementary materials for more details).

Next, we investigated the scope of the ring contraction with respect to the nature of the α-aroyl group (Fig. 3B). Here, the reaction was shown to be sensitive to sterics, with *p*-methyl substitution (**5a**) giving rise to higher yields and diastereoselectivity compared with the isomeric *o*-methyl–substituted **5b**. Aryl ketones featuring electron-donating substituents, such as ethers (**5c**) and thioethers (**5d**), led to good yields and diastereoselectivity for the desired product. Halogen-containing α-aryl-ketone **5e** was also competent in the ring contraction chemistry, affording an additional functional handle for modification after ring contraction. By comparison, electron-withdrawing groups such as *p*-CN and *p*-CF_3 (e.g., **5f** and **5g**) led to the formation of the desired product in modest yield and lower diastereoselectivity. This is likely the result of the increased acidity of the α-keto-proton in the product, which could undergo epimerization. On the basis of our calculations, epimerization through a retro–Mannich-Mannich pathway is unlikely (vide infra). Additionally, in the case of substrate **5g**, we observed an ensuing ring opening of the product through Norrish type II cleavage, evidencing the potential overreactivity of the cyclopentane products in some cases (see the supplementary materials for more details). Other aromatic ketones were also examined. For example, extended aromatic systems such as naphthalenyl ketones (**5h**) performed comparably, as did heteroaromatics such as thiophenyl ketones (see **5k**). Although the conditions identified were optimized for α-aroyl groups, several substrates bearing non–aryl-substituted ketones also participated successfully in the ring contraction transformation. Specifically, the desired products were observed for an alkynyl C(sp)–bearing substrate (**5l**) and a vinyl C(sp^2)–bearing substrate (**5m**). In the case of **5l**, the substantial decrease in yield can be attributed to a competing Norrish–Yang cyclization process leading to an azetidinol side product (see the supplementary materials for more details). Using more forcing, higher-energy (mercury lamp) irradiation, alkyl C(sp^3)–substituted ketone **5n** was converted to **6n** in 25% yield, highlighting, even in this case, the differential reactivity of the ketone groups in the starting material and product.

Substituted piperidines and several other saturated heterocycles were then examined for their propensity to undergo this type of ring contraction (Fig. 3C). Single substituents at the γ-position were tolerated (see **7a**), imparting stereocontrol. Benzannulated substrates such as tetrahydroisoquinoline **7b** successfully underwent the ring contraction transformation, providing the corresponding amino indane scaffolds (i.e., **8b**) in good yields and under mild conditions. Additionally, upon irradiation of substrates containing a morpholine scaffold, the tetrahydrofuran heterocycle (**8c**) was formed. The ring contraction methodology was also

extended beyond azacyclic frameworks to α-acylated thiane and tetrahydropyran derivatives. These were also competent substrates, leading to the formation of cyclopentane thiol and alcohol products (see **8d** to **8h**), respectively. In the case of **7d**, formation of the resulting thiol (**8d**) could be viewed as the unveiling of a covalent modifier upon photoirradiation.

Finally, we turned our attention toward the application of the ring contraction methodology to biologically active small molecules to demonstrate the potential for late-stage derivatization of drug candidates. Upon irradiation, MDMC (**9a**, stimulant), rimiterol (**9b**, bronchodilator), cathinone (**9c**, DAT reuptake inhibitor) (31), and mefloquine (**9d**, anti-malarial) derivatives underwent contraction to their corresponding cyclopentane isomers (Fig. 4A). In the case of **9d**, a ring-opened aldehyde side product was also observed, potentially arising from hydrolysis of the imine intermediate before Mannich-type ring closure. We speculate that these events were likely due to the electron-deficient bis-trifluoromethylquinoline group in **9d**. The ring contraction transformation was also leveraged in peptide diversification (Fig. 4B). Here, glycine-containing peptide **11** was converted to the corresponding amino cyclopentane (**12**), unveiling an H-bond donor. In this example, irradiation converts the α-peptide grouping to the corresponding β-amino ketone, accomplishing a nonintuitive peptide modification. Prospective applications include unveiling peptide-turn mimics upon irradiation.

Because of the participation of cyclic ether derivatives in these light-mediated ring contractions, we also explored this rearrangement in sugar editing (Fig. 4C). When subjected to 400-nm irradiation conditions, D-galactose–derived bis-acetonide **13** gave isomeric ring–opened product **14**. Here, the enol resulting from the Norrish type II ring opening presumably tautomerizes to the aryl ketone and does not engage the lactone carbonyl group, offering a powerful targeted “digestion” of sugar derivatives.

Computational insight

To gain insight into the proposed mechanism and origin of stereoselectivity for these photomediated ring contractions, we performed a computational study for the reaction of *N*-tosyl piperidine derivative **3b** (Fig. 5A). All of the quantum chemical calculations in the transition state modeling presented were performed using the Gaussian 16 program (32). Geometry optimizations and frequency calculations were performed at the M06–2X/6–31+G** level of theory with the SMD model for implicit solvation by benzene (see the supplementary materials for more details) (33–35). We initially postulated that the positional selectivity for 1,5-HAT could be attributed to the greater hydricity and lower bond dissociation energy of the α-amino hydrogen atom (Fig. 5A, ^{3}**3b** → ^{3}**A**). Using density functional theory (DFT) calculations, we found that the more hydridic and polarity matched α-piperidinyl hydrogen atom had a HAT transition state 9.0 kcal/mol lower in energy than the potentially competing C–H abstraction at the γ-position (36, 37). The calculations also revealed a conformational preference in the transition state for the N–S bond wherein maximal separation is maintained between the carbonyl and sulfonyl oxygens (see the supplementary materials for more details).

We also reasoned that the diastereoselective formation of the *cis*-disposed amino cyclopentane products (e.g., **4b**) would potentially result from a series of noncovalent interactions such as π-stacking and H-bonding in the transition state for the Mannich-type ring closure. Computed transition state structures support the Mannich-type cyclization/C–C bond formation proceeding in concert with proton transfer from the enol moiety to the *N*-tosyl group, consistent with the proposal by Suárez and co-workers for the aldol-type cyclization in hexopyranose carbohydrates (22). Three scenarios could be envisaged that qualitatively support the experimentally observed diastereoselectivity (Fig. 5C, top right). In the first scenario, only the (*E*/*Z*) imine–enol is productive. This geometry arises when fragmentation of diradical intermediate ^{3}**A** occurs faster than acyl bond rotation (Fig. 5A, see ^{3}**A** orange bond). Alternatively, if interconversion of the (*Z*) and (*E*) forms for both the enol (C=C) and the imine (C=N) bonds is facile, then all four possible imine–enol double-bond geometries can be accessed in the Mannich cyclization. However, the requisite triplet 1,4-diradical conformer that would afford the (*Z*)-imine (Ts-axial) is high in energy, and the contributions from a (*Z*)-imine geometry to the stereochemical outcome are expected to be negligible (see the supplementary materials for a complete discussion). We propose, therefore, that the most likely scenario is one in which the diradical is long-lived enough to allow acyl bond rotation and subsequent sampling of both enol diastereomers (38, 39). In this scenario, only the (*E*/*Z*) and (*E*/*E*) imine–enols are accessible and the energy differences between **TS-1–4** would determine the stereochemical outcome. The Boltzmann average of these four transition states predicted a ratio of 14:1 in favor of the *cis* cyclopentane isomer, in good agreement with the experimentally determined 12:1 ratio. The *cis* diastereoselectivity mainly originates from the energy difference between **TS-3** and **TS-4**, which could be rationalized by a shorter and presumably stronger H-bond, as well as a more staggered arrangement of substituents about the forming C–C bond in **TS-3** (Fig. 5C, ^{1}**B**→^{1}**4b**). The overall transformation of *N*-tosyl piperidine **3b** to either cyclopentane product was calculated to be exergonic (−4.2 kcal mol^{-1} for the **4b** compared with −3.3 kcal mol^{-1} for the *trans*-isomer of **4b**).

Insight into the selective reactivity of the starting material compared with the product under the reaction conditions was also supported by the DFT-calculated and empirically measured absorption profiles of **3b** and **4b**. Even though the calculated λ_{max} values for the starting material and product (Fig. 5B, top) did not differ markedly, we observed secondary absorption peaks associated with the expected n→π* occurring from 300 to 375 nm (Fig. 5B, bottom). Here, a hypsochromic shift was observed for amino cyclopentane product **4b** relative to starting piperidine **3b**, likely accounting for the selective excitation of the starting material. Also observed empirically was an overall decrease in absorptivity for the product (e.g., ε_{340} = 48.0 L cm^{-1} mol^{-1} for **3b** versus ε_{320} = 19.2 L cm^{-1} mol^{-1} for **4b**). Although predictions and rationalizations of photochemical processes tend to focus on λ_{max} values, in our system, irradiation at λ_{max} would have led to indiscriminate reaction of both the starting materials and products. By focusing on the secondary, n→π* absorption region of 300 to 375 nm, we were able to modulate the reactivity of the ketone group that is conserved in both the starting material and product by exploiting subtle differences in the absorbance wavelengths and extinction coefficients (see the supplementary materials for more details) (40). The emission spectrum of the 400-nm light source slightly overlaps with

the wavelength of light absorbed by the starting material but negligibly with the product. However, the empirically established optimal use of a commercially acquired 400-nm blue LED light source remains to be fully reconciled with the measured absorption values.

Toward a general asymmetric variant

Our insights into the observed diastereoselectivity for these transformations, which arises from highly organized transition states of an achiral imine-enol intermediate (as revealed from our calculations), combined with the successes of other powerful enantioselective photomediated processes (41, 42), inspired us to pursue enantioselective variants. We observed the formation of racemic product **4b** when enantioenriched **3b** was subjected to the ring contraction conditions, confirming that in this formal radical polar crossover the imine–enol intermediate is achiral. Therefore, we could circumvent the inherent challenges associated with stereocontrol of radical intermediates by effecting enantioselective closure of the achiral imine-enol intermediate under a two-electron reaction manifold (43). Given the ample literature precedent and predictive models for chiral phosphoric acid–catalyzed reactions of imines, we postulated that rate enhancement of the Mannich step would occur after imine protonation and attendant deprotonation of the enol, leading to an organized transition state favoring attack on one enantioface (see Fig. 6 and the supplementary materials for more details). The combination of H-bonding and ion pairing that would be realized in this case was anticipated to yield enantioenriched Mannich products (Fig. 6) (44–48).

Consistent with this hypothesis, ring contraction of **3b** with 10 mol% of (*R*)-TRIP (CPA1) as an additive provided (−)-**4b** in 92:8 enantiomeric ratio (e.r.) 84% enantiomeric excess (*ee*) with yields and diastereoselectivity consistent with those obtained under the standard reaction conditions for the formation of the racemate; using the SPINOL-derived phosphoric acid (*R*)-XYL-SPA (CPA2) gave (+)-**4b** in 95:5 e.r. (90% *ee*). Enantioselectivity, albeit modest, was also observed for amide, urea, THIQ, morpholine, and tetrahydropyran derivatives, giving rise to the enantioenriched products **4m, 4s, 8b, 8c, 8e**, and **8g**, respectively.

Conclusion

Using a Norrish type II reaction, we have established a versatile method for the scaffold remodeling of piperidines as well as other saturated heterocycles. The overall transformation is robust, and the conditions tolerate a wide range of functional groups. Key to the success of these transformations is the “photo-protection” of a pendant ketone group in the product through intramolecular H-bonding, an observation supported by our experimental and computational findings. This reaction has been rendered enantioselective using chiral phosphoric acids.

Supplementary Material

Refer to Web version on PubMed Central for supplementary material.

ACKNOWLEDGMENTS

We acknowledge the help and support of the following people from Merck Sharp & Dohme Corp., a subsidiary of Merck & Co., Inc., Kenilworth, NJ, USA (MSD): S. W. Krska, D. DiRocco, T. W. Lyons, D. Lehnherr, L.-C. Campeau, A. Northrup, N. K. Terrett, E. R. Parmee, and M. H. Kress for support of the Disruptive Chemistry Fellowship program; U. F. Mansoor and E. Corcoran for assistance with flow chemistry; J. Sauri and E. Kwan for assistance in NMR structure elucidation; D. Lehnherr, M. Uehling, D. Kalyani, and S. Lin for assistance with high-throughput experimentation; Y. Jiang, T. Johnson, R. Ayore, and W. Pinto for collecting HRMS data; L. M. Nogle, D. A. Smith, A. Beard, M. Darlak, and M. Pietrafitta for reversed-phase purifications; S. McMinn and L. Nogle for chiral SFC purifications; and N. Sciammetta, A. Musacchio, and E. Corcoran for thorough review of the manuscript and helpful discussions. We also thank A. Reeves for collecting UV-Vis data and J. Roque and J. S. Ham (Berkeley) for their helpful discussions.

Funding:

This work was supported by the Disruptive Chemistry Fellowship program of MSD (to C.S.Y.); the MRL Postdoctoral Research Program of MSD (to M.C.L.); the National Institutes of Health (grant S100D024998 funding the 600-MHz cryoprobe). R.S. is grateful to the NSF under the CCI Center for Selective C–H functionalization (grant CHE-1700982) and the National Institute of General Medical Sciences (grant R35GM130345A) for partial support of the work reported herein (Berkeley).

Data and materials availability:

All reported data can be found in the manuscript or the supplementary materials. Requests for additional materials should be directed to the corresponding authors. X-ray crystallographic data for **3a, 4a, 4m, 9a, 10a**, and (−)-**4b** (CCDC 2061160, 2061161, 2061162, 2061169, 2061170, and 2071240, respectively) are available from the Cambridge Crystallographic Data Centre (https://www.ccdc.cam.ac.uk/).

REFERENCES AND NOTES

1. Vitaku E, Smith DT, Njardarson JT, J. Med. Chem 57, 10257–10274 (2014). [PubMed: 25255204]
2. Lawrence AS, Amines: Synthesis, Properties and Applications (Cambridge Univ. Press. 2004).
3. Coldham I, Leonori D, Org. Lett 10, 3923–3925 (2008). [PubMed: 18683935]
4. Campos KR, Klapars A, Waldman JH, Dormer PG, Chen C-Y, J. Am. Chem. Soc 128, 3538–3539 (2006). [PubMed: 16536525]
5. Seel S et al., J. Am. Chem. Soc 133, 4774–4777 (2011). [PubMed: 21388211]
6. Chen W, Ma L, Paul A, Seidel D, Nat. Chem 10, 165–169 (2018). [PubMed: 29359746]
7. Pastine SJ, Gribkov DV, Sames D, J. Am. Chem. Soc 128, 14220–14221 (2006). [PubMed: 17076471]
8. Jain P, Verma P, Xia G, Yu J-Q, Nat. Chem 9, 140–144 (2017). [PubMed: 28282045]
9. Roque JB et al., ACS Catal. 10, 2929–2941 (2020). [PubMed: 33569242]
10. Millet A et al., Chem. Sci 4, 2241–2247 (2013).
11. Oeschger R et al., Science 368, 736–741 (2020). [PubMed: 32409470]
12. Topczewski JJ, Cabrera PJ, Saper NI, Sanford MS, Nature 531, 220–224 (2016). [PubMed: 26886789]
13. Campos KR et al., Science 363, eaat0805 (2019). [PubMed: 30655413]
14. Tehrani KA et al., Tetrahedron Lett. 41, 2507–2510 (2000).
15. Feraldi-Xypolia A, Gomez Pardo D, Cossy J, Chemistry 21, 12876–12880 (2015). [PubMed: 26218227]
16. Roque JB, Kuroda Y, Göttemann LT, Sarpong R, Nature 564, 244–248 (2018). [PubMed: 30382193]
17. Wang F, He Y, Tian M, Zhang X, Fan X, Org. Lett 20, 864–867 (2018). [PubMed: 29345128]
18. Ling R, Mariano PS, J. Org. Chem 63, 6072–6076 (1998). [PubMed: 11672222]

19. Wang S, Wang H, Tian N, Yan H, Tetrahedron Lett. 65, 152797 (2021).
20. Gees T, Schweizer WB, Seebach D, Helv. Chim. Acta 76, 2640–2653 (1993).
21. Álvarez-Dorta D, León EI, Kennedy AR, Riesco-Fagundo C, Suárez E, Angew. Chem 120, 9049–9051 (2008).
22. Álvarez-Dorta D et al., Chemistry 19, 10312–10333 (2013). [PubMed: 23788424]
23. Brameld KA, Kuhn B, Reuter DC, Stahl M, J. Chem. Inf. Model 48, 1–24 (2008). [PubMed: 18183967]
24. Anslyn EV, Dougherty DA, "Photochemistry" in Modern Physical Organic Chemistry, Anslyn EV, Dougherty DA, Eds. (University Science Books, 2006), pp. 935–1000.
25. Oelgemöller M, Hoffmann N, Org. Biomol. Chem 14, 7392–7442 (2016). [PubMed: 27381273]
26. Reichardt C, Welton T, "Solvent effects on the position of homogeneous chemical equilibria," in Solvents and Solvent Effects in Organic Chemistry, Reichardt C, Welton T, Eds. (Wiley, 2010), pp. 107–163.
27. Zheng Q et al., Chem. Soc. Rev 43, 1044–1056 (2014). [PubMed: 24177677]
28. Dave R, Terry DS, Munro JB, Blanchard SC, Biophys. J 96, 2371–2381 (2009). [PubMed: 19289062]
29. van der Velde JHM et al., Faraday Discuss. 184, 221–235 (2015). [PubMed: 26449795]
30. Wuts PGM, Greene TW, "Protection for the amino group," in Greene's Protective Groups in Organic Synthesis, Greene TW, Ed. (Wiley, ed. 4, 2006), pp. 696–926.
31. Yadav-Samudrala BJ, Eltit JM, Glennon RA, ACS Chem. Neurosci 10, 4043–4050 (2019). [PubMed: 31369229]
32. Frisch MJ et al., "Gaussian 16, Revision A.3" (Gaussian, 2016).
33. Zhao Y, Truhlar DG, Theor. Chem. Acc 120, 215–241 (2008).
34. Marenich AV, Cramer CJ, Truhlar DG, J. Phys. Chem. B 113, 6378–6396 (2009). [PubMed: 19366259]
35. Ribeiro RF, Marenich AV, Cramer CJ, Truhlar DG, J. Phys. Chem. B 115, 14556–14562 (2011). [PubMed: 21875126]
36. Padwa A, Tetrahedron Lett. 5, 3465–3469 (1964).
37. Walling C, Gibian MJ, J. Am. Chem. Soc 87, 3361–3364 (1965).
38. Abe M, Chem. Rev 113, 7011–7088 (2013). [PubMed: 23883325]
39. Muthukrishnan S et al., J. Org. Chem 75, 1393–1401 (2010). [PubMed: 20113004]
40. Staveness D, Collins JL 3rd, McAtee RC, Stephenson CRJ, Angew. Chem. Int. Ed 58, 19000–19006 (2019).
41. Brimioulle R, Bach T, Science 342, 840–843 (2013). [PubMed: 24233720]
42. Hölzl-Hobmeier A et al., Nature 564, 240–243 (2018). [PubMed: 30542163]
43. Sibi MP, Manyem S, Zimmerman J, Chem. Rev 103, 3263–3296 (2003). [PubMed: 12914498]
44. Verkade JMM, Hemert LJC, Quaedflieg PJLM, Rutjes FPJT, Chem. Soc. Rev 37, 29–41 (2008). [PubMed: 18197331]
45. Li JS, Liu YJ, Li S, Ma JA, Chem. Commun 54, 9151–9154 (2018).
46. Yang GF et al., J. Org. Chem 86, 5110–5119 (2021). [PubMed: 33724032]
47. Reid JP, Simón L, Goodman JM, Acc. Chem. Res 49, 1029–1041 (2016). [PubMed: 27128106]
48. Reid JP, Sigman MS, Nature 571, 343–348 (2019). [PubMed: 31316193]

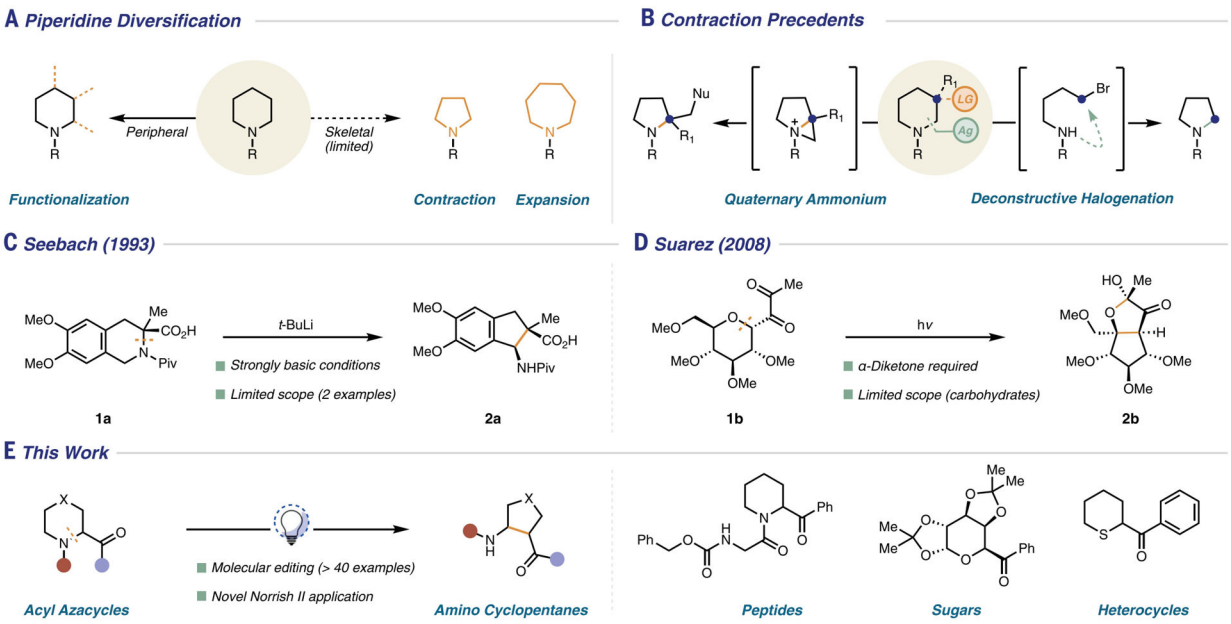

Fig. 1. Approaches to piperidine diversification.

(**A**) Peripheral functionalization and skeletal remodeling. (**B**) Selected examples of ring contractions on piperidine frameworks. (**C**) Seminal report of Seebach and co-workers' unusual THIQ ring contraction (20). (**D**) Contraction of carbohydrates reported by Suárez and co-workers (21). (**E**) Norrish type II approach to piperidine skeletal framework modification (this work).

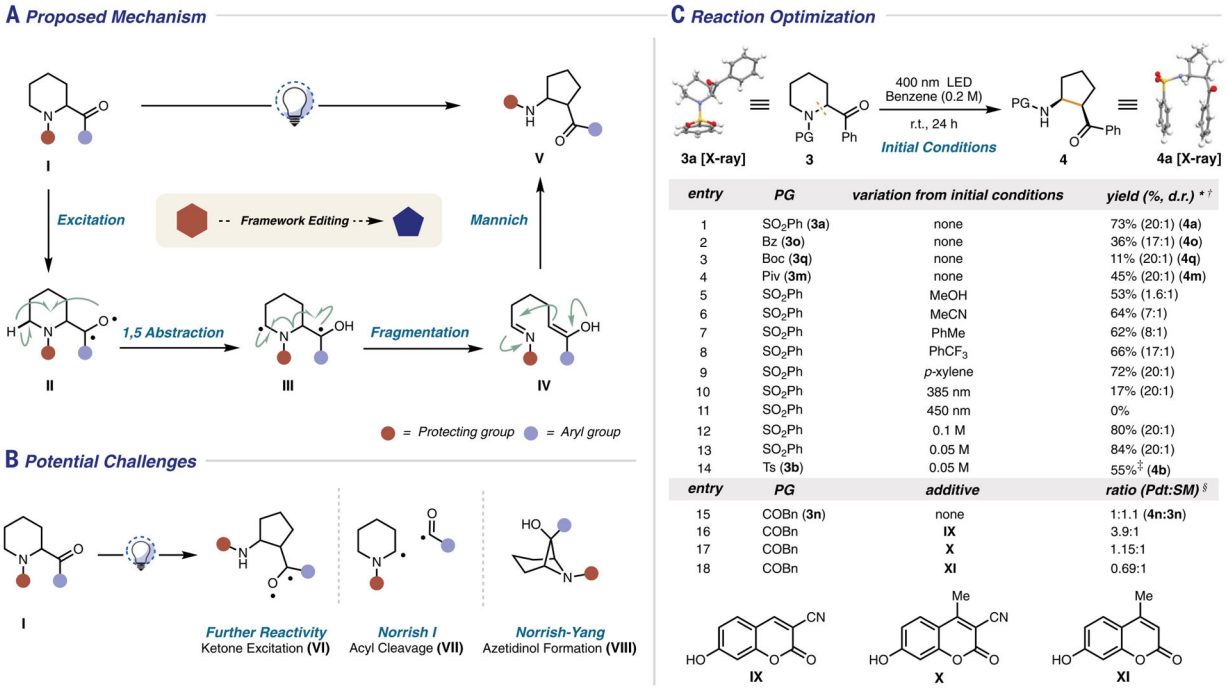

entry	PG	variation from initial conditions	yield (%, d.r.) *†
1	SO_2Ph (**3a**)	none	73% (20:1) (**4a**)
2	Bz (**3o**)	none	36% (17:1) (**4o**)
3	Boc (**3q**)	none	11% (20:1) (**4q**)
4	Piv (**3m**)	none	45% (20:1) (**4m**)
5	SO_2Ph	MeOH	53% (1.6:1)
6	SO_2Ph	MeCN	64% (7:1)
7	SO_2Ph	PhMe	62% (8:1)
8	SO_2Ph	$PhCF_3$	66% (17:1)
9	SO_2Ph	*p*-xylene	72% (20:1)
10	SO_2Ph	385 nm	17% (20:1)
11	SO_2Ph	450 nm	0%
12	SO_2Ph	0.1 M	80% (20:1)
13	SO_2Ph	0.05 M	84% (20:1)
14	Ts (**3b**)	0.05 M	55%‡ (**4b**)
entry	**PG**	**additive**	**ratio (Pdt:SM) §**
15	COBn (**3n**)	none	1:1.1 (**4n:3n**)
16	COBn	**IX**	3.9:1
17	COBn	**X**	1.15:1
18	COBn	**XI**	0.69:1

Fig. 2. Reaction development.

(**A**) Proposed mechanism for piperidine ring contraction. (**B**) Potential undesired side reactivity through Norrish type I and Norrish–Yang cyclization processes. (**C**) Reaction optimization for light-mediated ring contraction. Reactions were performed on a 0.05 mmol scale. Relative stereochemistry is depicted. *Yields were determined by ^{1}H NMR integration using Ph_3CH as an internal standard. †Diastereomeric ratio (d.r.) was determined by ^{1}H NMR integration of resonances corresponding to diastereomers in the crude mixture. ‡Reaction was performed on a 1-g scale in flow, with an isolated yield of major diastereomer reported. §High throughput experimentation (HTE) conducted to identify 3-cyanoumbelliferone. Conversion was determined by liquid chromatography–mass spectrometry analysis.

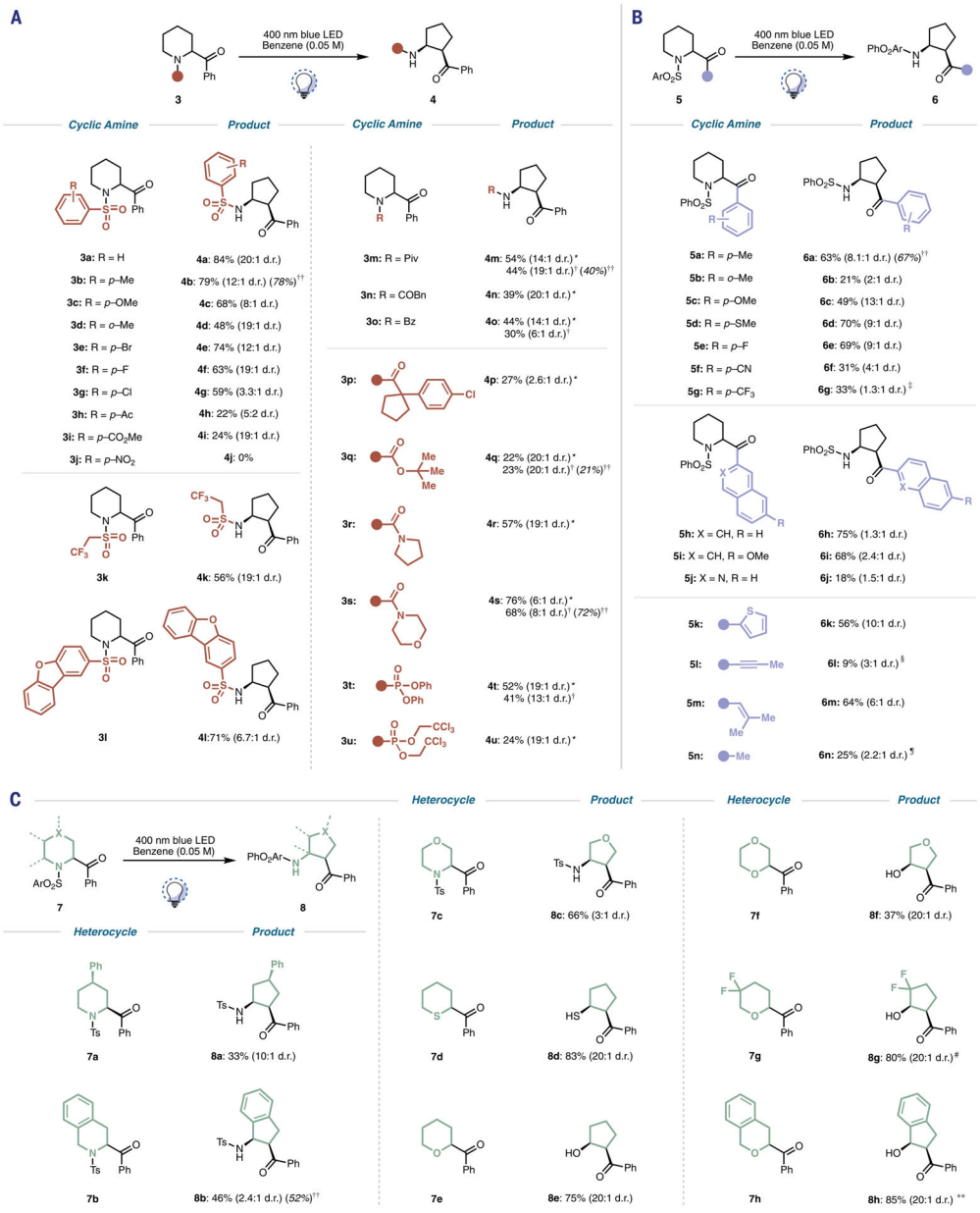

Fig. 3. Scope of substrates in piperidine ring contraction.

Reaction conditions: Starting material (0.2 mmol), benzene (0.05 M), 400 nm LED, 18 to 24 hours. Isolated yields reported and relative stereochemistry are shown. Diastereomeric ratio was determined by ^{1}H NMR integration of resonances corresponding to diastereomers in the crude. (**A**) Scope of protecting groups in ring contraction. *Additive **IX** (30 mol%) was added to the reaction mixture. †0.2 mmol scale trials conducted in the absence of additive **IX**. (**B**) Scope of aryl ketone in ring contraction. ‡Ring-opened product after a subsequent Norrish type II process is also observed. §(With *N*-Ts) Norrish–Yang azetidinol product observed in 12% (19% *brsm*). ¶(With *N*-Ts) Reaction irradiated with a medium-pressure mercury lamp for 24 hours. (**C**) Scope of heterocyclic core in ring contraction. #Reaction conducted on a 0.14 mmol scale. **Reaction conducted on a 0.11 mmol scale. ††Selected

examples conducted on a 0.05 mmol scale using *p*-xylene (0.05 M) as a solvent. Yield was determined by ^{1}H NMR integration using Ph_3CH as an internal standard (see the supplementary materials for more details).

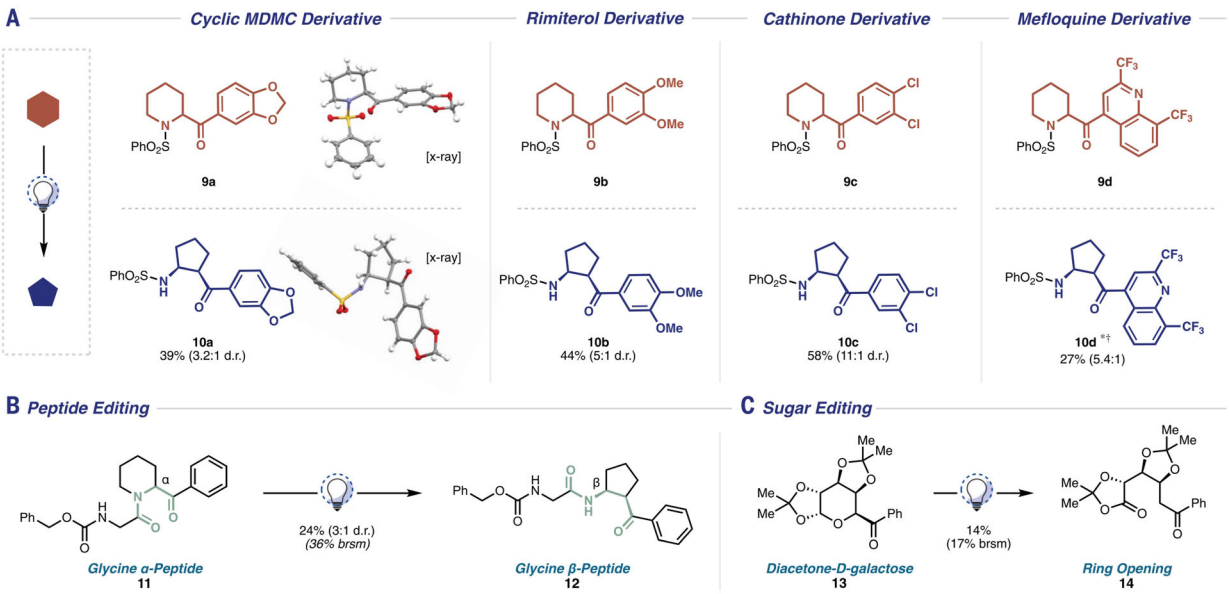

Fig. 4. Applications toward biologically relevant compounds.

(**A**) Selected examples of bioactive drug molecule contraction. (**B**) Ring contraction–mediated peptide editing (see the supplementary materials for more details). (**C**) Sugar editing enabled by targeted "digestion." Reaction conditions: Starting material (0.2 mmol), benzene (0.05 M), 400 nm LED, 24 hours. Isolated yields reported and relative stereochemistry are shown. Diastereomeric ratio was determined by ^{1}H NMR integration of resonances corresponding to diastereomers in the crude. *Reaction conducted on a 0.1 mmol scale, where yield was determined by ^{1}H NMR integration using Ph_3CH as an internal standard and d.r. was determined by ^{1}H NMR integration of resonances corresponding to diastereomers in the crude. †Ring-opened product also observed in 4.5% yield (see the supplementary materials for more details).

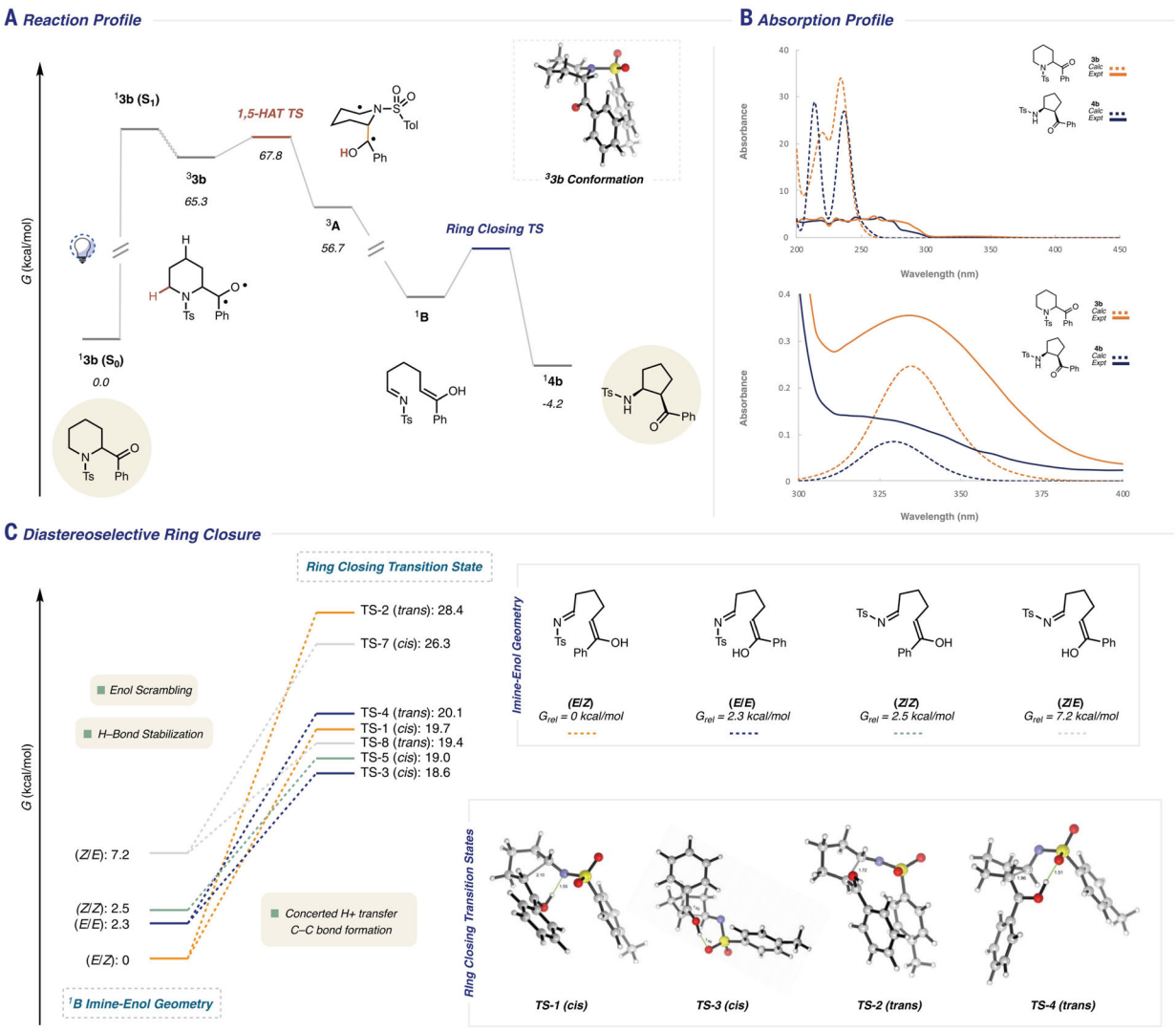

Fig. 5. Computational studies on ring contraction mechanism.

(**A**) Reaction profile for the piperidine ring contraction. (**B**) Experimentally and computationally (normalized) determined absorption profiles for the starting material (**3b**) and product (**4b**). (**C**) Imine-enol geometries and transition states calculated for the diastereoselective ring closure.

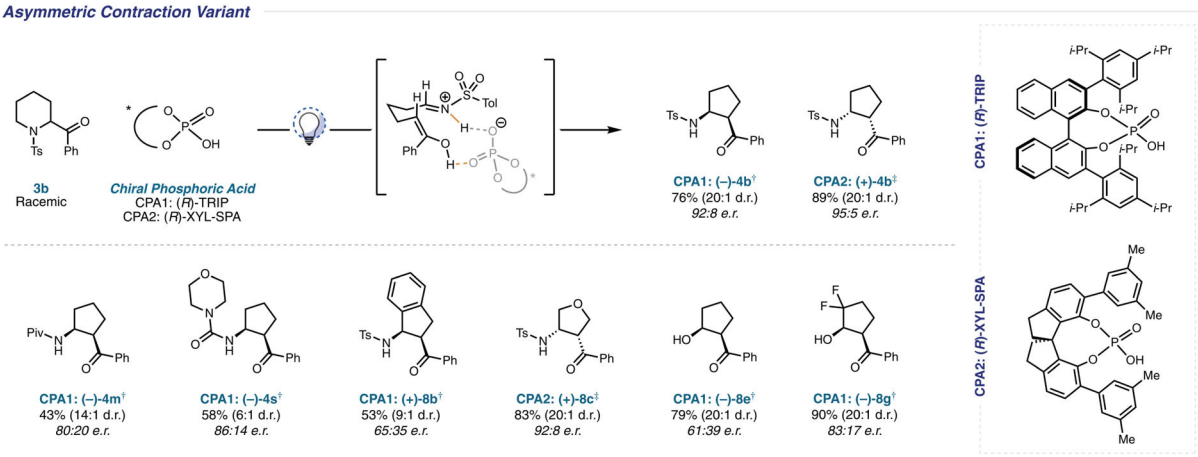

Fig. 6. Development of an asymmetric ring contraction variant.

*Reaction conducted on a 0.05 mmol scale in which yields were determined by ^{1}H NMR integration using Ph_3CH as an internal standard and d.r. was determined by ^{1}H NMR integration of resonances corresponding to diastereomers in the crude. For the major diastereomer, e.r. was determined by SFC analysis. †10 mol% (*R*)-TRIP (CPA1) used as chiral phosphoric acid. ‡10 mol% (*R*)-XYL-SPA (CPA2) used as chiral phosphoric acid.